Biophysical Journal, Volume *114*

Supplemental Information

Dehomogenized Elastic Properties of Heterogeneous Layered Materials in AFM Indentation Experiments

Jia-Jye Lee, Satish Rao, Gaurav Kaushik, Evren U. Azeloglu, and Kevin D. Costa

The original Eshelby homogenization theory (1) was modified by Li et al. to encompass the full range of inclusion volume fraction ($0 \leq f_{\Omega} \leq 1$) using modified Eshelby tensor terms derived for spherical inclusions within a finite domain (2). Example effective Young's modulus (E_{eff}) vs. f_{Ω} curves based on the original and modified Eshelby theories are shown in **Figure S1A**, for arbitrarily selected values of the elastic modulus (E_M = 10 kPa and E_{Ω} = 100 kPa) and the Poisson's ratio ($\upsilon_M = \upsilon_{\Omega} = 0.49$) for the substrate and inclusion, respectively. Compared to the modified theory, the original Eshelby theory only agreed within the first 15% of the inclusion volume fraction range, consistent with the sparse inclusion condition for which homogenization theory was originally developed. We also compared the modified Eshelby model with the Hashin-Shtrikman variational approach, which predicts lower and upper bounds on the effective elastic modulus of a composite material with arbitrary interface geometry given the elastic properties and inclusion volume fraction of the material constituents (3). The modified Eshelby model fell within the limits of the Hashin-Shtrikman model throughout the full range of the inclusion volume fraction (**Figure S1B**). This supported our incorporation of the modified Eshelby homogenization theory into our hybrid Eshelby decomposition (HED) approach to analyze AFM indentation of composite samples with layered heterogeneity.

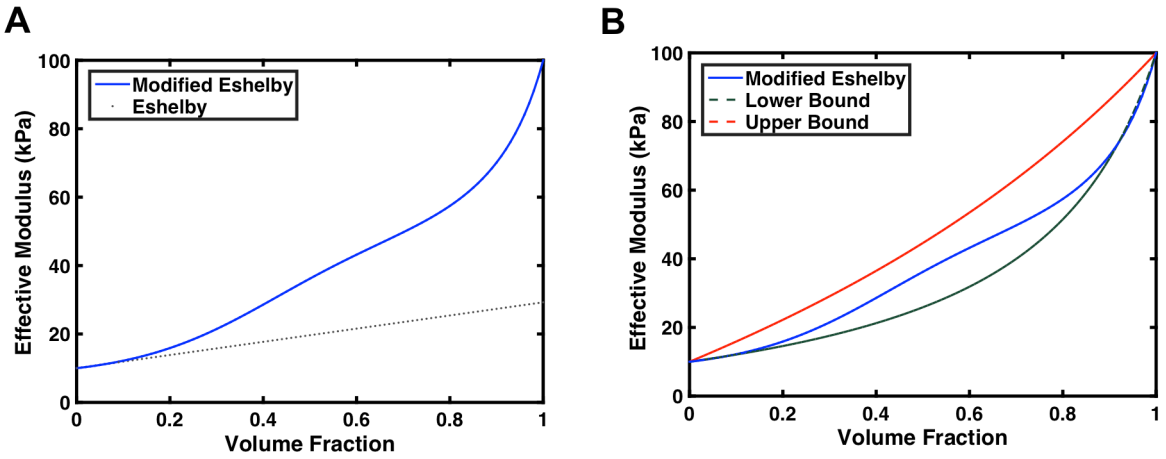

Figure S1: Comparison of homogenization theories: (**A**) Li's modified Eshelby theory for finite inclusions diverges from Eshelby's original homogenization theory when the inclusion volume fraction exceeds about 15%. (**B**) Over the full range of inclusion volume fractions, the modified Eshelby theory falls within the upper- and lower-bounds predicted by the Hashin-Shtrikman model for arbitrary finite inclusions.

For any arbitrary two-component sample with known elastic properties of the inclusion and substrate (e.g., E_{inc} = 100 kPa, E_{sub} = 10 kPa, υ_{inc} = υ_{sub} = 0.49), the effective modulus vs. volume fraction relationship can be calculated using Equation (11) from the modified Eshelby homogenization theory (**Figure S2A**). For a specific hypothetical example using these modulus values, AFM indentation of a layered sample with a stiff (100-kPa) 3-μm top layer on a soft (10-kPa) 50-μm substrate using a 25-μm spherical probe was modeled by FEM, and pointwise analysis of the simulated force-depth response (4) was used to obtain the effective elastic modulus vs. indentation depth (**Figure S2B**). From these two curves, the effective inclusion volume fraction vs. indentation depth (f_{eff} vs. D) relationship is readily obtained at matched values of E_{eff}, using a simple local linear interpolation algorithm as needed to match the modulus values exactly. For instance, in the above example the pointwise effective modulus equals 15 kPa at a depth of 2 μm (**Figure S2B**), while the same effective modulus of 15 kPa corresponds to an inclusion volume fraction of 0.2 based on the Eshelby equation (**Figure S2A**). Therefore, for this model, the effective inclusion volume fraction is 0.2 at an indentation depth of 2 μm. Proceeding through all the indentation depths, the volume fraction vs. indentation depth curve is readily constructed without ambiguity (**Figure S2C**). A somewhat unexpected empirical finding that is critical to the HED approach is that for a given indenter geometry and layered sample configuration, the f_{eff} vs. D curve is relatively insensitive to the specific layer and substrate modulus values, hence giving rise to the concept of a "master curve" as presented in Figures 4 and 5 in the Results. This means that a PDMS sample with a soft 3-μm thick top layer on a stiff 50-μm substrate has essentially the same f_{eff} vs. D relationship as a 3-μm soft intima on a 50-μm stiff media. This has practical value because layer thickness is readily measured by microscopy or other means, while the layer-specific elastic modulus values are typically the unknown desired quantities in biological applications of AFM indentation.

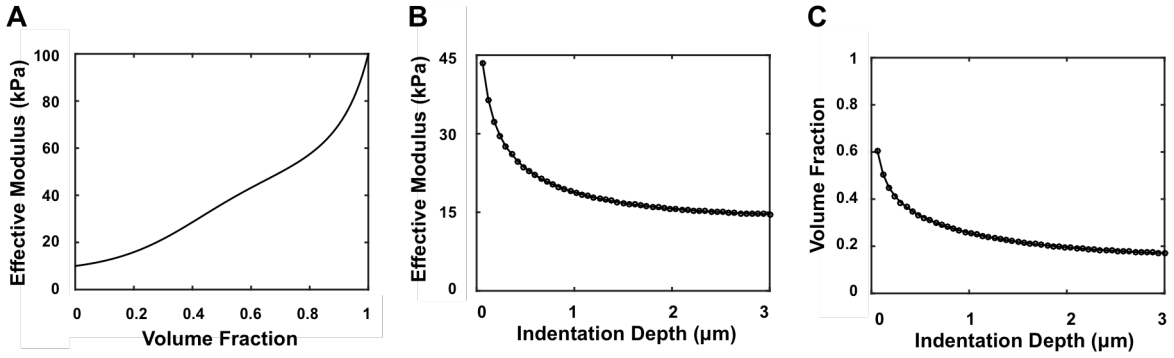

Figure S2: (A) Effective modulus vs. volume fraction, (B) effective (i.e., pointwise) modulus vs. depth, and (C) effective volume fraction vs. depth obtained by combining data from panels A and B at matched values of effective modulus.

To examine the robustness of the HED approach in the presence of uncertainty or variability in tissue dimensions, we analyzed synthetic data using intentionally inaccurate layer thickness values to determine the effects on the reconstructed layer-specific elastic moduli. Finite element modeling was used to simulate a 25-μm diameter AFM tip indenting a 4-μm thick, 3-kPa top inclusion layer on a 10-kPa bottom substrate, with data spanning about 40% of the full volume fraction range. HED analysis was then performed using master curves corresponding to 3-, 4-, 5-, 6-, and 7-μm thick top layers, introducing under- and over-estimation of the top layer thickness. The reconstructed modulus values for the bottom layer were 9.5, 9.8, 10.6, 10.6, and 11.2 kPa, respectively, and the reconstructed modulus values for the top layer were 2.4, 2.8, 3.4, 3.5, and 3.9 kPa, respectively. Thus, errors in the top-layer thickness appear to have a greater effect on the estimated values of the top-layer modulus (blue squares), while the substrate modulus (red circles) appears less sensitive to thickness errors (**Figure S3**). For the most severe case in the simulation (i.e., assuming a 7-μm layer thickness instead of the true 4-μm thickness) the 75% error in thickness yielded a 30.8% error in modulus of the top layer, and a 11.7% error in the bottom layer modulus. More typical errors in thickness related to tissue fixation, on the order of 10%, are therefore likely to introduce similar errors in the HED-reconstructed modulus values, which is comparable to the experimental uncertainty of the AFM measurements.

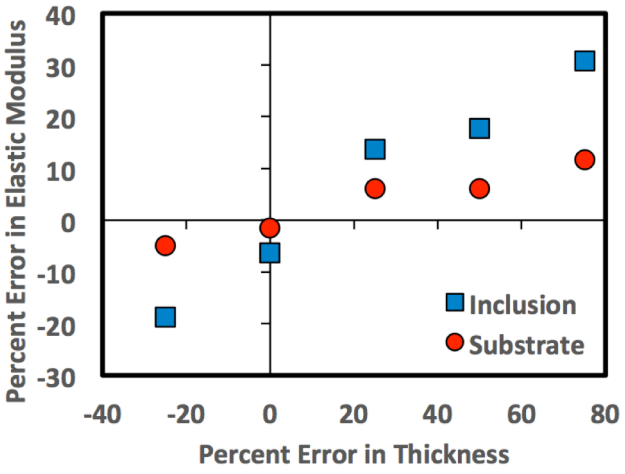

Figure S3: Estimated error in HED-reconstructed inclusion and substrate elastic modulus values for a layer sample due to errors in the assigned thickness of the top layer.

To evaluate the effects of a restricted data set limited to a portion of the full range of inclusion volume fractions ($0 \leq f_{eff} \leq 1$), Monte Carlo simulation including 10% random noise was used to generate 1000 synthetic data sets from the FEM of indentation of a 100-kPa inclusion layer on a 10-kPa substrate. The f_{eff} data were restricted to sub-ranges between 0.2 and 0.8 prior to fitting with the Eshelby curve to estimate the values of substrate and inclusion moduli, E_{sub} and E_{inc}. The distributions of estimated moduli were quantified in terms of the percent error of the interquartile range (IQR), calculated from the 50% confidence interval relative to the true assigned values. In **Figure S4**, each color bar spans the included sub-range of f_{eff} on the x-axis, and the resulting percent error is color-coded with darker colors indicating smaller errors in the estimated elastic modulus values.

In general, a wider sub-range of volume ratio and a smaller lower-bound of the sub-range (corresponding to deeper indentations) yielded more accurate estimates of E_{sub} (**Figure S4A**) and E_{inc} (**Figure S4B**). In the figure below, the bottom group with sub-ranges starting at $f_{eff} = 0.2$ generated ~8% error in E_{sub} and E_{inc}, and the error tended to increase as the upper-end value of the f_{eff} sub-range was reduced, narrowing the data range. The error also tended to increase as the lower-end value of the f_{eff} sub-range groups increased to 0.3 or 0.4. Including a small lower-end value of the f_{eff} contributed to better estimation of E_{sub} even with a slightly smaller width of the sub-range (**Figure S4A**). For example, the 0.3-0.6 sub-range generated ~12% error in E_{sub} versus ~16% error in the 0.4-0.8 sub-range, and the group starting with f_{eff} equal to 0.2 at the lower-end yielded < 8% error in E_{sub} even with a sub-range width of just 30% of the full range (i.e., 0.2-0.5).

Similarly, the approximation of E_{inc} improved with a larger upper-end value of f_{eff}, but also depended strongly on the lower-end value of the sub-range (**Figure S4B**). To illustrate this, the 40%-wide sub-ranges of 0.4-0.8, 0.3-0.7, and 0.2-0.6 yielded ~13%, ~10%, and ~9% errors in E_{inc}, respectively. The 0.4-0.8 sub-range extended closest to the pure inclusion limit ($f_{eff} = 1$) but resulted in higher error in E_{inc} (and in E_{sub}) than the other two ranges. This indicated that coverage of lower inclusion volume fractions, achieved with deeper indentations during an AFM experiment, is a priority for accurate modulus estimation by HED analysis. Therefore, we conclude that data covering a sub-range width of at least 30% of the lower portion of the full f_{eff} range, excluding the two extreme ends of the range that tend to be unachievable in practice, allowed robust reconstruction of E_{sub} and E_{inc} even in the presence of random noise, with improved accuracy as the f_{eff} sub-range width increases.

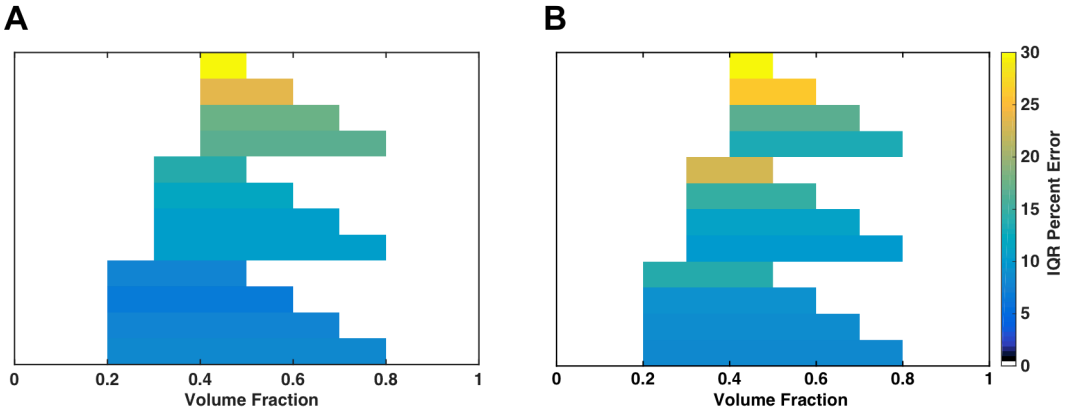

Figure S4: Monte Carlo simulation of the percent error in the 50% inter-quartile range (IQR) of reconstructed (**A**) substrate modulus E_{sub}, and (**B**) inclusion modulus E_{inc}, for different sub-ranges of the effective inclusion volume fraction, f_{eff}.

The pointwise modulus (E_{pw}) distribution of a SOFT inclusion bi-layer started high as the indention began, decreased as the indenter moved down to the softer inclusion layer, and then increased as the indenter compressed the stiffer bottom substrate (**Figure S5A**). According to HED analysis, the extracted elastic moduli of top inclusion and bottom substrate were 276.1 kPa and 130.3 kPa, respectively. We suspected that a thin stiff surface film, possibly related to the polymer-air interface during the PDMS curing process, might have caused the stiff behavior at the onset of indentation. To clarify this speculation, a FEM four-layer model was created with a 500-nm surface film (3 MPa) on top of a 5-μm thick inclusion (60 kPa) and an interface film with the same properties between the soft inclusion and the stiffer (200 kPa) substrate layer. The FEM simulated a 15-μm spherical probe indenting 3-μm deep into the four-layer model. Analysis of the simulated force-depth data showed depth-dependent E_{pw} similar to the AFM experiment; the four-layer model skewed the E_{pw} and increased overall stiffness in comparison to the corresponding bi-layer model without stiff films (**Figure S5B**). Scanning electron microscope (SEM) imaging of the cross-section of a bi-layered PDMS sample confirmed the presence of a thin top surface layer and a thin interface layer (**Figure S5C**), consistent with the hypothesized thin films created during the two-step curing process of the bi-layer sample.

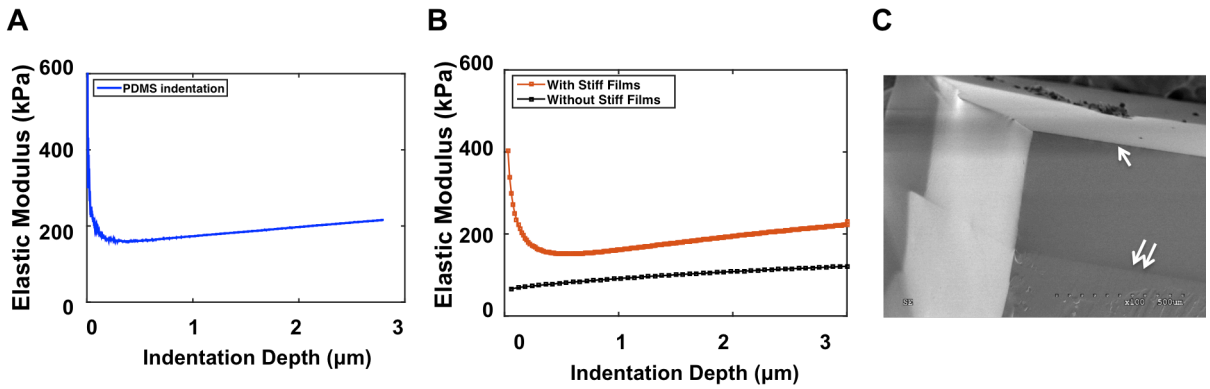

Figure S5: Representative elastic modulus vs. depth curve of (**A**) an AFM experiment on the SOFT PDMS bi-layer sample, (**B**) simulated four-layered FEM model of 60-kPa inclusion and 200-kPa substrate without (black) and with (red) 5-MPa stiff films, in which the latter showed similar behavior to experimental data in panel A. (**C**) SEM image of a bi-layer PDMS sample showed two film structures, one at the top surface (single arrow) and one at the bi-layer interface (double arrows).

A representative HED analysis of AFM indentation of a FLAT mouse aorta configuration is demonstrated below. The indentation force vs. depth relationship was obtained from each force curve (**Figure S6A**). The pointwise analysis (4) was then used to obtain an apparent elastic modulus vs. indentation depth curve from each force-depth pair, revealing depth-dependent changes in elastic modulus that reflect heterogeneity of the sample material properties (**Figure S6B**); a pointwise elastic modulus that starts low at shallow depths and increases as the probe indents deeper suggests a composite sample with a soft layer on top of a stiffer substrate. The master curve for a SOFT configuration with 3-μm top layer and 35-μm substrate, defining the effective inclusion volume fraction (f_{eff}) vs. indentation depth (gray line, **Figure S6C**), was then combined with the pointwise modulus to obtain the modulus vs. volume fraction relationship at matched indentation depths (**Figure S6D**); the included data spanned a 30% volume fraction range of 0.3-0.6 (black data points in **Figure S6C**), reflecting an indentation depth of 0.54 to 1.56 μm (the shaded regions in **Figures S6A and S6B)**. Fitting the modulus vs. volume fraction data with the modified Eshelby theory (2) yielded estimates of the substrate modulus (at $f_{eff} = 0$) and inclusion modulus (at $f_{eff} = 1$), corresponding to E_{med} (41.2 kPa) and E_{int} (4.1 kPa), respectively (**Figure S6D**). In this demonstration, the HED analysis included a volume fraction range of about 0.3 to 0.6 (30% coverage) and showed a robust reconstruction of media and intima elastic properties consistent with the overall mean values of E_{med} (37.45 ± 6.29 kPa) and E_{int} (6.64 ± 0.78 kPa) obtained in this study (see **Figure 9** in main text).

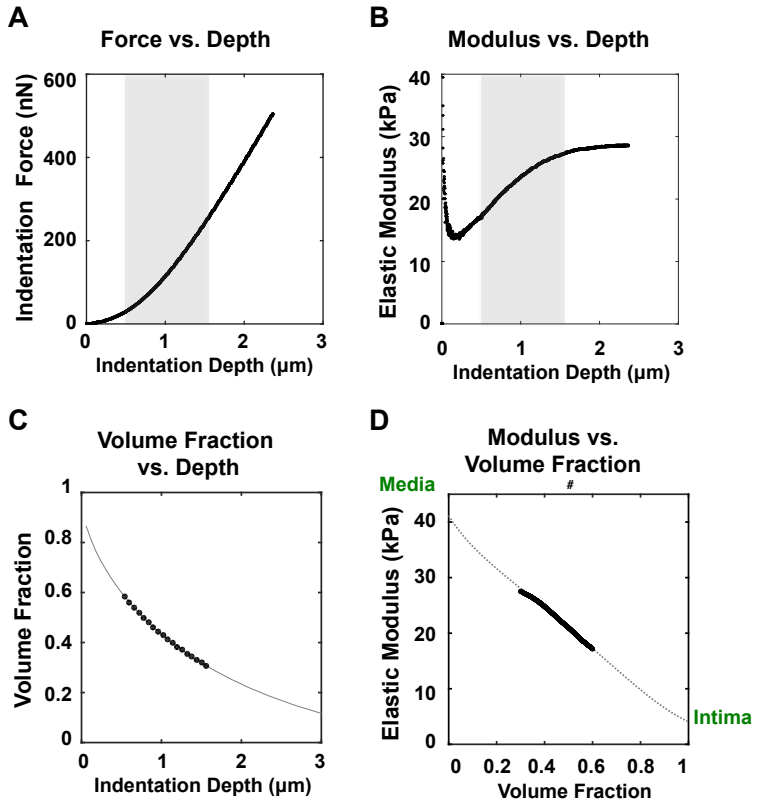

Figure S6: Representative experimental AFM indentation responses on wild type mouse abdominal aorta in the FLAT configuration, showing (**A**) indentation force vs. depth, (**B**) pointwise elastic modulus vs. depth, (**C**) inclusion volume fraction vs. depth, and (**D**) the resulting modulus vs. volume fraction (f_{eff}) curve used to extract the layer-specific aorta elastic properties, E_{med} = 41.2 kPa (f_{eff} = 0) and E_{int} = 4.1 kPa (f_{eff} = 1), for the media and intima, respectively. Note that the shaded regions (0.54-1.56 μm) in panels (A) and (B) correspond to the inclusion volume fraction range of 0.3-0.6 in panels (C) and (D).

As mentioned in the Discussion, Sokolov and coworkers accounted for the steric interaction with a soft superficial brush structure to improve estimation of elastic properties of a stiffer cellular material underlying a surface layer of glycoproteins and membrane protrusions (5, 6), but the biophysics of this model is fundamentally different than our case of bonded elastic layers, where penetration of the top layer does not occur. The Sokolov study also showed that the substrate modulus can be estimated by neglecting the brush region of the indentation response and fitting the elastic Hertz model only to the deepest indentation data. Other investigators have used a similar approach to examine depth-dependent changes in elastic properties of biological samples (7). This is similar to the Linearized-Hertz approach of Kaushik et al. (8), in which bi-layer properties of a soft-on-stiff sample are extracted by neglecting the transition zone and selectively fitting the Hertz model to the shallow-indentation and deep-indentation regimes. To test the efficacy of this approach compared to HED analysis, the FEM was used to simulate AFM indentation using a 25-μm spherical probe, and a bi-layer sample with a 3-μm thick top layer in either a SOFT inclusion configuration (1-kPa layer on a 10-kPa substrate) or a STIFF inclusion configuration (100-kPa layer on a 10-kPa substrate). As shown in **Figure S7A and B**, for the SOFT inclusion case, when the Hertz-type model was restricted to the initial 10% of the indentation range (0 to 0.3 μm) or the final 10% of the indentation range (2.7 to 3.0 μm), the estimated modulus values were E_{inc} = 3.65 kPa and E_{sub} = 7.90 kPa, respectively. Using the same approach for the STIFF inclusion case (**Figure S7D and E**), the estimated modulus values were E_{inc} = 29.50 kPa and E_{sub} = 12.32 kPa. In comparison, the HED analysis yielded E_{inc} = 1.27 kPa and E_{sub} = 9.60 kPa for the SOFT layer configuration (**Figure S7C**), and E_{inc} = 90.66 kPa and E_{sub} = 10.01 kPa for the STIFF layer configuration (**Figure S7F**). Thus, although the modified Hertz approach was able to distinguish the soft-on-stiff from the stiff-on-soft heterogeneity configurations, accuracy of the estimated layer-specific modulus values was markedly improved using the HED analysis.

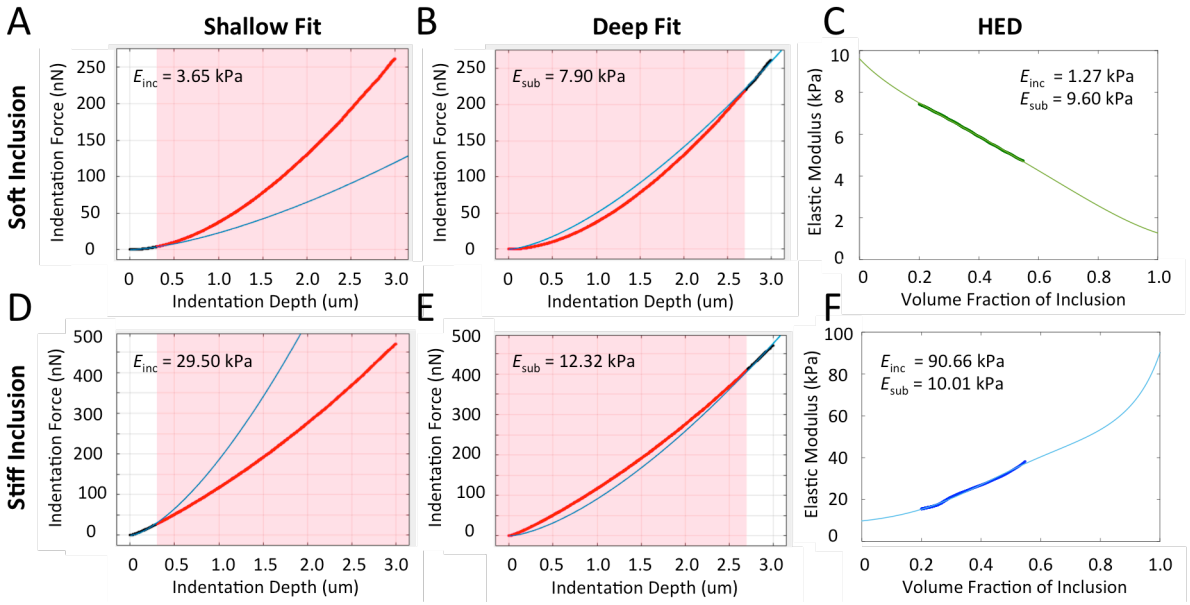

Figure S7: Comparison of Hertz-type (**A, B, D, E**) and HED (**C, F**) analysis methods for SOFT (**A, B, C**) and STIFF (**D, E, F**) layer inclusion configurations simulated using FEM (see text for details). Thick lines and symbols represent the FEM data, thin lines represent model fits. White region in Hertz-type graphs shows subregion of data used for fitting.

Supporting References

1. Eshelby, J. D. 1957. The determination of the elastic field of an ellipsoidal inclusion, and related problems. Proc. R. Soc. A 241:376-396.
2. Li, S., R. Sauer, and G. Wang. 2005. A circular inclusion in a finite domain I. The Dirichlet-Eshelby problem. Acta Mechanica 179:67-90.
3. Hashin, Z., and S. Shtrikman. 1963. A variational approach to the theory of the elastic behaviour of multiphase materials. J Mech Phys Solids 11:127-140.
4. Costa, K. D., and F. C. Yin. 1999. Analysis of indentation: implications for measuring mechanical properties with atomic force microscopy. J. Biomech. Eng. 121:462-471.
5. Dokukin, M. E., N. V. Guz, and I. Sokolov. 2013. Quantitative study of the elastic modulus of loosely attached cells in AFM indentation experiments. Biophysical Journal 104:2123-2131.
6. Guz, N., M. Dokukin, V. Kalaparthi, and I. Sokolov. 2014. If cell mechanics can be described by elastic modulus: study of different models and probes used in indentation experiments. Biophysical Journal 107:564-575.
7. Rotsch, C., K. Jacobson, and M. Radmacher. 1999. Dimensional and mechanical dynamics of active and stable edges in motile fibroblasts investigated by using atomic force microscopy. Proc. Natl. Acad. Sci. USA 96:921–926.
8. Kaushik, G., A. Fuhrmann, A. Cammarato, and A. J. Engler. 2011. In situ mechanical analysis of myofibrillar perturbation and aging on soft, bilayered drosophila myocardium. Biophys J. 101:2629–2637.